

# Unsupervised Part Discovery by Unsupervised Disentanglement

Sandro Braun   Patrick Esser   Björn Ommer

Heidelberg Collaboratory for Image Processing / IWR, Heidelberg University  
{first name}.{last name}@iwr.uni-heidelberg.de

**Abstract.** We address the problem of discovering part segmentations of articulated objects without supervision. In contrast to keypoints, part segmentations provide information about part localizations on the level of individual pixels. Capturing both locations and semantics, they are an attractive target for supervised learning approaches. However, large annotation costs limit the scalability of supervised algorithms to other object categories than humans. Unsupervised approaches potentially allow to use much more data at a lower cost. Most existing unsupervised approaches focus on learning abstract representations to be refined with supervision into the final representation. Our approach leverages a generative model consisting of two disentangled representations for an object’s shape and appearance and a latent variable for the part segmentation. From a single image, the trained model infers a semantic part segmentation map. In experiments, we compare our approach to previous state-of-the-art approaches and observe significant gains in segmentation accuracy and shape consistency<sup>1</sup>. Our work demonstrates the feasibility to discover semantic part segmentations without supervision.

## 1 Introduction

Instances of articulated objects such as humans, birds and dogs differ in their articulation (different pose) and also show different colors and textures (appearance). Despite those large variations in articulation and appearance, humans are able to establish correspondences between individual parts across instances.

For example, consider two persons wearing different outfits as in Fig. 1a. One is wearing a plain, blue shirt, the other one is wearing a dotted, white T-shirt. In the first case, arms and chest share the same appearance, thus information about appearances cannot be used to identify the parts. In the second case, arms and chest have different appearances, thus information about appearances could be used to identify the parts.

Most previous approaches for learning part segmentations are based on supervised learning. While this can lead to good performance on a narrow set of object classes, especially that of humans [10], it requires to build a large dataset for each object of interest. To overcome this limitation, we require methods that

---

<sup>1</sup> Code available at <https://compvis.github.io/unsupervised-part-segmentation>



(a) Two people with similar poses,  $\pi_1 \simeq \pi_2$ , but different appearances  $\alpha_1 \neq \alpha_2$ . Semantic segmentations  $S_1, S_2$  are unaffected by appearance variations, i.e.  $S_1 \simeq S_2$ , and thus independent thereof.

(b) In our model, the joint distribution over images  $x$ , segmentations  $S$ , poses  $\pi$ , and appearances  $\alpha$  factorizes into  $p(x, S, \pi, \alpha) = p(x|S, \alpha)p(S|\pi)p(\pi)p(\alpha)$ . Thus,  $S$  is independent of  $\alpha$  and dependent on  $\pi$ . While  $\pi$  is a latent representation of pose,  $S$  is a semantic segmentation.

Fig. 1: **A probabilistic model for unsupervised part discovery.** As illustrated in a), semantic segmentations are appearance independent, which is reflected in the structure of our probabilistic model shown in b).

discover parts and their segmentations solely from observing the data, i.e. we need unsupervised approaches.

Previous works on unsupervised keypoint discovery [14, 25, 48] produce semantic keypoints which could provide information about parts. However, as we show in our experiments, even when combined with image intensity information to estimate the shape of parts, inferring pixel-wise localizations of parts from keypoints remains ambiguous. An essential ingredient of keypoint-based approaches is the built-in low-dimensional bottleneck which encourages compression and hence learning. The keypoints are represented through heatmaps of spatially normalized activations, which encourages well localized activations i.e. keypoints. In contrast, a segmentation of parts has roughly the same dimensionality as the image itself and allows arbitrary shapes of the segmented parts. Thus we cannot use the segmentation as a built-in bottleneck and must find a different way to enforce the bottleneck.

To learn parts and their segmentation unsupervised, we propose a probabilistic generative model with three hidden variables. We use two low-dimensional, continuous variables, which are independent of each other, to disentangle the instance-specific appearance, from the instance-invariant shape. The third variable is a high-dimensional discrete variable to model the support of parts, hence a segmentation. It is a descendant of the appearance-independent shape variable to ensure independence of instance specific appearance. We show how the mask can be efficiently learned in a variational inference framework assuming suitable priors. Overall, our approach learns to infer a semantic part segmentation map

from a single image by learning from a stream of video frames or from pairs of synthetically transformed images.

In experiments on multiple datasets of humans and birds, our method is able to discover parts within the image that are consistent across instances. We compare intersection-over-union metrics (IOU) of our approach to those obtained from previous methods on keypoint learning and observe improvements in two out of three datasets of humans and on the dataset of birds. In addition, the generative nature of our approach enables part-based appearance transfers where it outperforms both pose supervised and keypoint-based unsupervised approaches in terms of shape consistency.

## 2 Background

*Disentangled Representation Learning* To learn more meaningful representations, [6, 35] build upon the Variational Autoencoder (VAE) [18, 34] to encourage disentanglement. However, non-identifiability issues [13, 24] suggest that additional information is required to obtain well-defined factors.

[19] demonstrated a factorization into style and content of digits using a conditional variant of the VAE. Motivated by Generative Adversarial Networks (GANs) [9], [27] adds a discriminator to this architecture. Using videos, [5] uses a classification problem to obtain disentangled representations of the temporally varying factors and its stationary factors. This approach is closely related to estimating and minimizing the Mutual Information of two factors [2] by defining the joint distribution of the two factors through samples from the same video.

*Localized Representation Learning* Image segmentation is a well studied problem in computer vision. The seminal work of [30] introduced a variational formulation to approximate images by piecewise constant functions with regularized edge length. Superpixel approaches [33] group nearby pixels according to their similarity and obtain oversegmentations of an image. [1] combines a hierarchy of segmentations with contour detection to improve results. However, these methods rely on low-level image features and cannot account for semantic similarity.

Co-segmentation assumes the availability of a large number of examples showing the object to be segmented. The ability of this paradigm to learn from such a weak source of information resulted in many different approaches [26] ranging from graphical models [41] to deep generative models [37]. But their underlying assumption that the object to be segmented is salient limits them to masks of a single object, whereas our method learns multiple semantic parts, with part-wise correspondences across instances.

*Unsupervised Part Discovery* Part based models have been extensively studied [29, 36, 40, 45]. Recent works demonstrated the ability to discover semantic keypoints without supervision. Based on the differentiable score-map to keypoint layer of [46], [38] learns keypoints which are stable under synthetic image transformations by enforcing an equivariance principle. [48] integrates this principle into an autoencoder framework. [14] uses a reconstruction task with two images from the

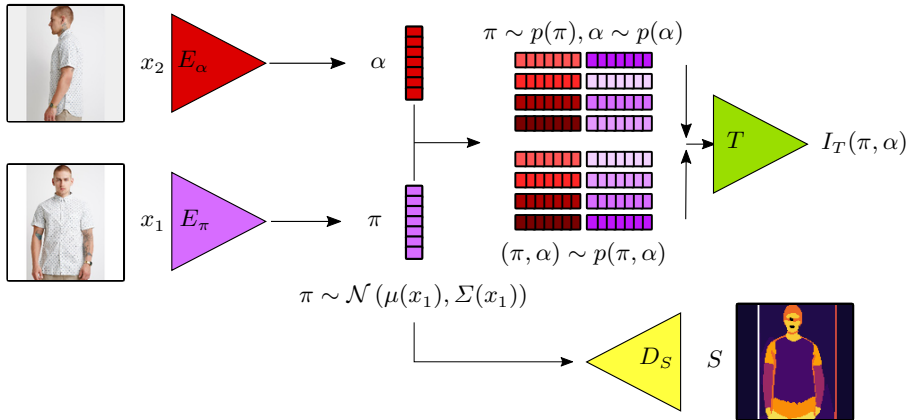


Fig. 2: **Learning Appearance Independent Segmentations.** To learn segmentations  $S$  independent to appearance variation  $\alpha$ , we first disentangle a global representation for shape  $\pi$  and appearance  $\alpha$ . The disentanglement is achieved through a variational and an adversarial constraint.

same video, instead of synthetic transformations. [25] makes the representation more expressive by considering ellipses instead of circles for keypoints. However, in all cases the intermediate representation of keypoints is crucial, We obtain pixel-accurate part memberships, whereas above approaches can only give a rough heatmap of part localizations. In addition, our approach can handle occlusions robustly which we demonstrate in our experiments.

### 3 Approach

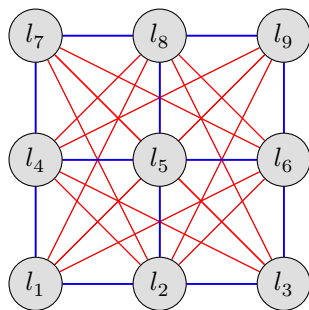
We have an image  $x$  depicting an object  $o$  composed of  $N$  object parts  $o_1, \dots, o_N$ . We would like to build a model that learns about those object parts and assigns each location in the image to its corresponding object part, thus a part segmentation. Without supervision for part segmentations, we rely on a generative approach by looking for the segmentation  $S^*$  that explains the image  $x$  best. Using Bayes rule, we can rewrite this as follows:

$$S^* = \arg \max_S p(S|x) = \arg \max_S p(x|S)p(S). \quad (1)$$

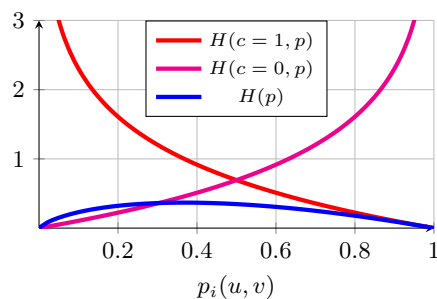
The likelihood  $p(x|S)$  measures if the segmentation can describe the image well enough and the prior  $p(S)$  measures if  $S$  is a suitable candidate for a segmentation. We now motivate suitable choices for the priors of  $S$  for part learning.

#### 3.1 Appearance Independence of Segmentations

Take two people spontaneously striking the same pose as depicted in Fig. 1a. The two people have the same pose  $\pi$ , but different appearances  $\alpha_1$  and  $\alpha_2$ . This



(a) **Gaussian Markov Random Field.** Without any prior assumptions, any image pixel is dependent on any other pixel, (**dense** connectivity). In a GMRF, we only allow adjacent pixels to interact (**sparse** connectivity).



(b) **Entropy Regularization.** To keep the learned segmentation  $S$  close to a categorical distribution, we regularize the entropy of part probabilities  $p_i(u, v)$ .

Fig. 3: **Segmentation Priors.** We assume two priors for our segmentation model.

generates two images  $x_1$  and  $x_2$  and we infer corresponding part segmentations  $S_1$  and  $S_2$ . Intuitively, the part segmentations  $S_i$  are independent of the variation of individual appearances, and as those people share the same poses, clearly the part segmentation of the image will be the same, i.e.  $S_1 = S_2$ . We argue that we can exploit this independence by modifying the image generation process so that segmentations are a result of pose and shape. We now consider  $\alpha$  and  $\pi$  as random variables. In a graphical model sense, the joint distribution over poses, appearances and segmentations should factorize as depicted in Fig. 1:  $p(x, S, \pi, \alpha) = p(x|S, \alpha)p(S|\pi)p(\pi)$ . Note that this directly reveals the corresponding motivation in (1). If we had access to the underlying shape and appearance variables that generate images  $x$ , we know that the part segmentation  $S$  must be dependent on shape  $\pi$ . In practice,  $\pi$  and  $\alpha$  are hidden variables and we must learn to infer them from observations  $x$ .

### 3.2 Learning Appearance Independent Segmentations

We now explain how we achieve a disentangled representation of shape and appearance. Let  $x_i \sim (\alpha_i, \pi_i)$  express that  $\alpha_i$  and  $\pi_i$  were the factors generating the image  $x_i$ . We then sample  $x_1 = (\alpha, \pi_1)$  and  $x_2 = (\alpha, \pi_2)$  from the dataset. In practice, this means that we need a pair of images depicting the same object but with varied poses. To infer the latent variables, we use two encoders.

$$E_\alpha : \mathbb{R}^{\dim(x)} \rightarrow \mathbb{R}^{\dim(\alpha)}, x \mapsto \alpha, \quad E_\alpha(x_2) = \alpha \quad (2)$$

$$E_\pi : \mathbb{R}^{\dim(x)} \rightarrow \mathbb{R}^{\dim(\pi)}, x \mapsto \pi, \quad E_\pi(x_1) = \pi \quad (3)$$

Here,  $\alpha$  and  $\pi$  are simple low-dimensional latent variables, each represented by a vector. Please refer to the appendix for implementation details. To keep  $\pi$  independent of  $\alpha$ , we simply keep  $\pi$  close to a standard normal distribution in a

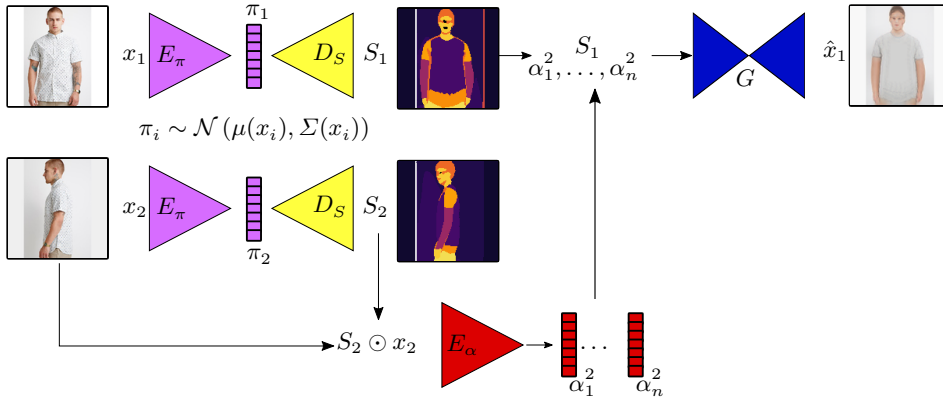


Fig. 4: **Complete Method.** First, we sample images  $x_1, x_2$  from the dataset and infer their segmentations  $S_1$  and  $S_2$ . We extract part based descriptors for appearance  $\alpha_1^2, \dots, \alpha_N^2$  from  $x_2$  by masking out each part using  $S_2$  and mapping it into appearance space using  $E_\alpha$ . We then build a likelihood model for  $x_1$  based on  $S_1$  and  $\alpha_1^2, \dots, \alpha_N^2$ .

variational framework, i.e.  $p(\pi) = \mathcal{N}(0, I)$  and  $q(\pi|x_1) = \mathcal{N}(\mu(x_1), \Sigma(x_1))$ . However, this is not sufficient to guarantee that  $p(\pi)$  is factorized into semantically consistent parts. To give an example, the model could also learn to factorize parts based on their average color, i.e. all blue parts and all red parts. To prevent this, we add an additional adversarial constraint that limits the mutual information between shape and appearance  $I(\alpha, \pi)$ . Following recent works on mutual information estimation [3, 28, 32], we achieve this through an adversary  $T$ , which is a simple classifier trained with the following objective

$$\max_T \mathbb{E}_{(\pi, \alpha) \sim p(\pi, \alpha)} \log(\sigma(T(\pi, \alpha))) + \quad (4)$$

$$\mathbb{E}_{\pi \sim p(\pi), \alpha \sim p(\alpha)} \log(1 - \sigma(T(\pi, \alpha))) \quad (5)$$

Here,  $\sigma(x)$  denotes the sigmoid activation. Intuitively, this means that we sample a batch of  $B$  image pairs,  $\{x_1^i, x_2^i\}$   $i = 1, \dots, B$ , from the dataset and map them through the encoders,  $\alpha = E_\alpha(x_2)$  and  $\pi = E_\pi(x_1)$ . This gives us a batch of samples from the joint distribution  $(\pi, \alpha)_i \sim p(\pi, \alpha)$ ,  $i = 1, \dots, B$ . We then randomly permute the order of  $\{\alpha_i\}$  within the batch to obtain a batch of samples from the marginal distribution  $\pi \sim p(\pi), \alpha \sim p(\alpha)$ .

The procedure is depicted in Fig. 2. Note that the procedure is not a classical image discriminator as used in a GAN [9] training, but rather a neural mutual information estimator [2, 7]. One can derive that in the limit, the adversary converges to an estimate of the mutual information. We thus term  $\mathbb{E}_{(\pi, \alpha) \sim p(\pi, \alpha)} T(\pi, \alpha) = I_T(\pi, \alpha) = \hat{I}(\pi, \alpha)$  an estimate for the mutual information of our disentangled representation. This summarizes the objectives used to train the encoders.

$$E_\pi : \min \mathcal{L}_{rec} + \lambda_{\text{variational}} \text{KL}(q(\pi|x) || p(\pi)) + \lambda_{\text{adversarial}} I_T(\pi, \alpha) \quad (6)$$

$$E_\alpha : \min \mathcal{L}_{rec} \quad (7)$$

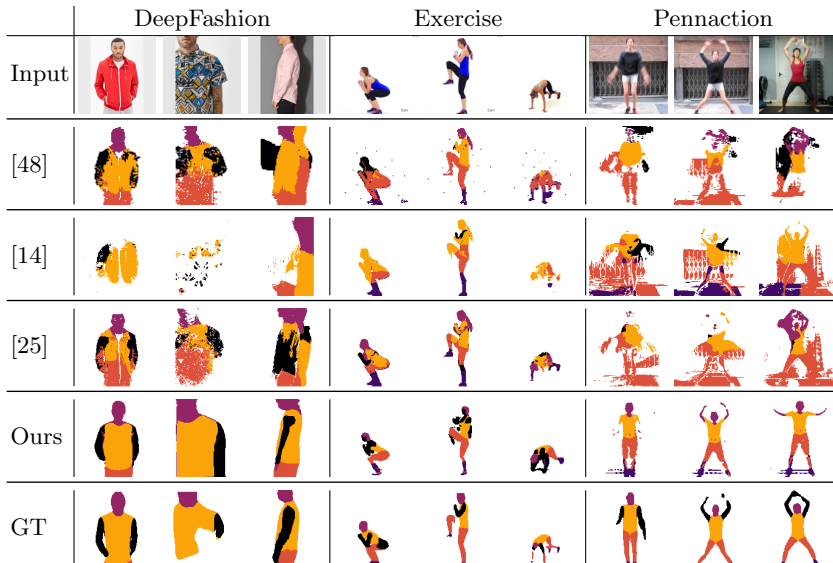


Fig. 5: **Qualitative Comparison Against Keypoint Learning.** To obtain segmentation masks from keypoint baselines, we use an unsupervised postprocessing based on a conditional random field [20]. We do not apply any postprocessing on our results.

Here  $\mathcal{L}_{rec}$  is a reconstruction likelihood, such as a  $\mathcal{L}_2$  loss or a perceptual loss between the original and the reconstructed image.  $\mathcal{L}_{rec}$  will be explained in more detail in Sec. 3.4. In practice, we rely on the adaptive regularization scheme proposed in [7].

Having a disentangled representation for shape and appearance, we can finally infer segmentations  $S$  given shapes  $\pi$  using a simple decoder model  $D_S$ . The full procedure of disentanglement and inference for segmentations is depicted in Fig. 2. However, without further prior knowledge, it is in general not clear that  $D_S$  will produce what resembles part segmentation under a common prior. We therefore need to formulate suitable priors for  $S$  to achieve the desired result.

### 3.3 Priors for Segmentations

This section motivates suitable priors for the segmentation  $S$ . We claim that part segmentations are locally smooth regions within the image, meaning that long-range interactions between pixels are only possible through local connectivity. We illustrate this high-level idea in Fig. 3a. To achieve local smoothness within the image, we interpret  $S$  as the output of a per-pixel classifier with probabilities  $p_i(u, v), i = 1, \dots, N$ . We obtain  $p_i(u, v)$  by a softmax normalization of the output of  $D_S$ , thus

$$D_S : \pi \mapsto l, \quad p_i(u, v) = \frac{\exp(l_i(u, v))}{\sum_{i=1}^N \exp(l_i(u, v))}. \quad (8)$$

Dataset	Method	Arms	Feet	Head	Legs	Torso	Overall
DeepFashion	[48] + CRF	0.194	0.000	0.598	0.293	0.376	0.292
DeepFashion	[14] + CRF	0.052	0.000	0.118	0.108	0.244	0.104
DeepFashion	[25] + CRF	0.215	0.000	<b>0.606</b>	0.309	0.322	0.290
DeepFashion	Ours	<b>0.508</b>	0.000	0.530	<b>0.500</b>	<b>0.722</b>	<b>0.452</b>
Exercise	[48] + CRF	0.043	<b>0.230</b>	0.096	0.433	0.335	0.227
Exercise	[14] + CRF	0.101	0.190	0.000	0.469	0.357	0.223
Exercise	[25] + CRF	0.212	0.213	<b>0.366</b>	<b>0.445</b>	0.441	<b>0.336</b>
Exercise	Ours	<b>0.253</b>	0.104	0.340	0.428	<b>0.504</b>	0.326
Pennaction	[48] + CRF	0.066	0.000	<b>0.327</b>	0.379	0.442	0.243
Pennaction	[14] + CRF	0.050	<b>0.122</b>	0.000	0.316	0.455	0.189
Pennaction	[25] + CRF	0.038	0.000	0.105	0.312	0.402	0.171
Pennaction	Ours	<b>0.094</b>	0.101	0.237	<b>0.371</b>	<b>0.484</b>	<b>0.257</b>

Table 1: **IOU Comparison Against Keypoint Learning.** To obtain segmentation masks from keypoint estimates, we use an unsupervised postprocessing based on a conditional random field [20]. See appendix for full details.

In practice,  $l$  can be seen as the logits of a classifier. We now assume a Gaussian Markov Random Field prior for  $l$ , i.e.  $p(l) = \mathcal{N}(0, \nabla)$ , where  $\nabla$  denotes the spatial gradient operator, which can be approximated using a finite-difference filter. To efficiently train  $D_S$ , we use variational inference, meaning that we are looking for a suitable approximate posterior. Using the mean-field approximation we can define  $q(l|x) = \prod_i^{\dim(l)} q(l_i|x) = \mathcal{N}(D_S(\pi), I)$ . Then, keeping  $l$  close to the chosen prior in a KL sense simply results in regularizing the spatial gradient.

$$\text{KL}(q||p) = \sum_{i=1}^N \sum_{u,v} \|\nabla_{(u,v)} l_i(u,v)\|^2 \quad (9)$$

Unfortunately, this prior is not sufficient. What is still missing is a prior that states that parts are mutually exclusive at every location, i.e. segmentations  $S$  are categorical. To enforce this, we have several options: using approximations of categorical distributions [4, 15], or add a regularizer that pushes the part segmentations towards a categorical solution, for instance by regularizing the entropy or cross-entropy, as shown in Fig. 3b. In practice, we found that entropy and cross-entropy regularization work best. For simplicity, we restrict us to the entropy regularization.

$$\min H(p) = \sum_{u,v} \sum_{i=1}^N p_i(u,v) \log p_i(u,v) \quad (10)$$

Here,  $(u,v)$  indicate spatial coordinate indices. To summarize, we employ the following objective for  $D_S$ .

$$D_S : \min \mathcal{L}_{rec} + \lambda_{\text{GMRF}} \text{KL}(q(l|x)||p(l)) + \lambda_{H(p)} H(p) \quad (11)$$

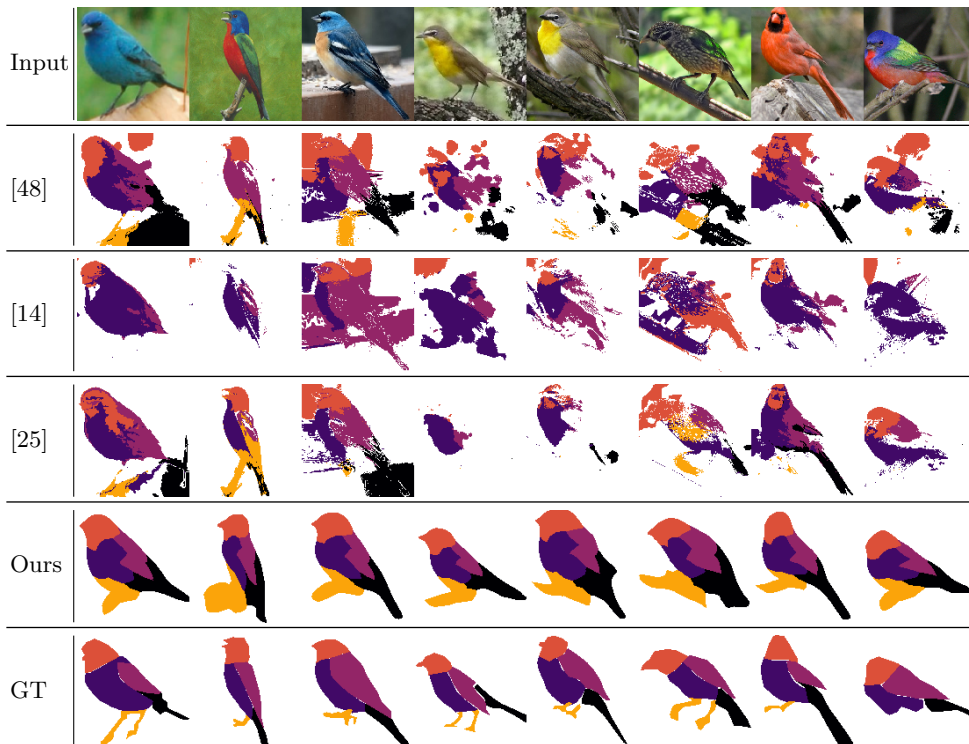


Fig. 6: **Qualitative Results on CUB.** Despite the lack of multi-view training pairs, we are still able to learn a good part model using our proposed method.

### 3.4 Part-based Image Generation

Having introduced all our chosen priors, it remains to specify the likelihood model  $p(x|S)$  i.e. how we generate images  $x$  from segmentations  $S$ . Clearly,  $S$  is not sufficient to explain the image because instance-specific appearance details are missing. We therefore would like to build a part-based likelihood model that adds instance-specific part appearances  $\alpha_i$ . We employ the following procedure, which is common practice in unsupervised keypoint learning [14, 25], as shown in Fig. 4.

1. Sample images  $x_1, x_2$  from the dataset and infer their segmentations  $S_1$  and  $S_2$ . As stated in Sec. 3.2,  $x_1$  and  $x_2$  are images of the same instance in different poses.
2. Extract part based descriptors for appearance  $\alpha_1^2, \dots, \alpha_N^2$  from  $x_2$  by masking out each individual part using  $S_2$  and mapping it into appearance space using  $E_\alpha$ . The masking out operation is a simple hadamard product of each inferred part segmentation  $x_{2,i} = S_{2,i} \odot x_2$  and can be interpreted as a part attention mechanism. We then obtain the part based descriptors using  $E_\alpha: \alpha_i^2 = E_\alpha(x_{2,i})$ .
3. We now have a set of vectors representing unlocalized part appearance descriptors and a spatial localization for those descriptors in terms of the segmenta-

Method	Head	Chest	Wing	Tail	Feet	Overall
[48] + CRF	0.207	0.320	0.318	0.365	0.074	0.257
[14] + CRF	0.000	0.394	0.158	0.189	0.000	0.148
[25] + CRF	0.203	0.477	0.347	0.431	0.068	0.305
Ours	<b>0.340</b>	<b>0.565</b>	<b>0.489</b>	<b>0.679</b>	<b>0.154</b>	<b>0.446</b>

Table 2: **IOU Comparison Against Keypoint Learning on Birds.** To obtain segmentation masks from keypoint baselines, we use an unsupervised postprocessing based on a conditional random field [20]. See appendix for details.

tion  $S$ . To bring back spatial information for the appearance descriptors  $\alpha_i^2$  we calculate the expected appearance descriptor at each pixel which we term  $S_\alpha$ :  $S_\alpha(u, v) = \sum_{i=1}^N \alpha_i^2 \cdot p_i(u, v)$

- Finally, we reconstruct the image  $x_1$  from  $S_\alpha$  using a generator network  $G$ . More formally, this gives us the part-based image likelihood.

$$p(x_1 | S_1, \alpha_1^2, \dots, \alpha_N^2) = \mathcal{N}(G(S_\alpha), I)(x_1) \quad (12)$$

With this approach, we make the assumption that part appearances are constant across all poses  $\pi$  for a specific instance. Then, minimizing the negative log-likelihood gives the  $\mathcal{L}_{rec}$  objective used in previous sections.

$$\mathcal{L}_{rec} = -\log(\mathcal{N}(G(S_\alpha), I)(x_1)) = \|G(S_\alpha) - x_1\|^2 \quad (13)$$

In practice  $G$  is a hour-glass style architecture [31] and  $\mathcal{L}_{rec}$  is implemented through a perceptual loss [16]. See supplementary for more details.

## 4 Experiments

*Human Object Category* We begin by evaluating our method on datasets of the human object category, namely DeepFashion [22, 23], Exercise [43, 44] and Pennaction [47]. DeepFashion contains strong variations in viewpoints, poses and appearances but only a simple background. Exercise has strong pose variation but only simple appearances and a simple background. Pennaction introduces the additional challenge of background clutter.

We evaluate the performance of our method using the intersection-over-union (IOU) metric against a ground-truth part annotation. We establish missing ground-truth annotation by using the supervised pretrained model from Densepose [10] as a substitute oracle. We calibrate our model on a held-out validation set to match the ground-truth as good as possible. Additional details can be found in the appendix.

We compare against recent work on unsupervised keypoint learning [14, 25, 48]. To compare keypoint learning with segmentation learning, we apply a conditional random fields (CRF) [20] postprocessing. This step is a standard technique to refine image segmentations [12, 39, 42]. Note that we *do not* apply any postprocessing on top of our proposed method. Additional details can be found in the appendix.

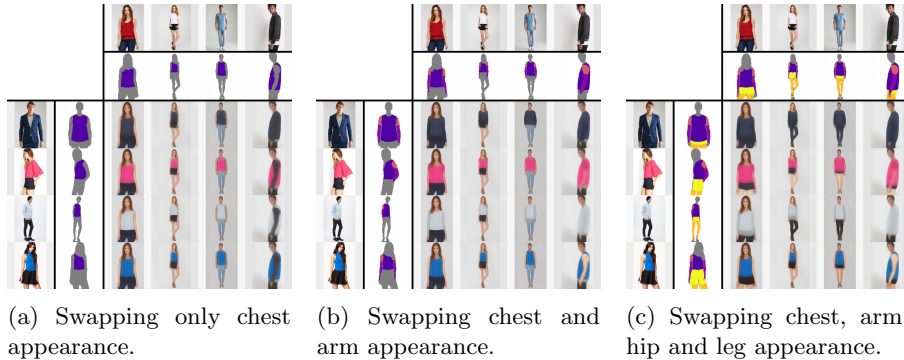


Fig. 7: **Part-based Appearance Transfer**. Parts which are swapped are highlighted in color (active), parts which remain constant are gray (inactive). (a): we transfer appearance of torso parts. (b): we transfer appearance of torso and arm parts. (c): we transfer appearance of torso, arm and leg parts. The transfer succeeds despite strong occlusions and viewpoint variations.

Qualitative results of our method and keypoint learning baselines [14, 25, 48] are shown in Fig. 5. We observe that keypoint consistency is especially difficult to achieve when dealing with strong viewpoint variations, for instance when switching between frontal and side poses on the DeepFashion and between push-up, squatting position on the Exercise dataset. The results on Pennaction suggest that background clutter is challenging for all methods, especially arm parts in downwards pointing poses. Note that on some images with an extreme amount of part occlusions, even the supervised ground-truth model by [10] fails to segment parts precisely (column 2, Fig. 5).

Finally, we show quantitative results in terms of IOU in Tab. 1. On DeepFashion and Pennaction our method outperforms other methods by a consistent margin in terms of IOU. On Exercise, the method is on par with the state-of-the-art keypoint model [25] paired with CRF postprocessing. The quantitative results validate our observation for all the datasets that our method is able to discover semantically consistent parts across instances in form of segmentations.

*Other Object Categories* We qualitatively analyze our method on the bird object category in Fig. 6. Note that CUB is a single image dataset, which requires us to use artificial thin-plate-spline transformations (TPS) as an approximation to multi-view pose variations. This approximation is identical to those used in [14, 25, 38]. We observe that our part discovery method learns local parts and is also able to find appropriate scales for parts for smaller sized birds. To evaluate our method quantitatively, we created a small dataset of bird part annotations as ground-truth information and evaluate against [14, 25, 48] in terms of IOU in Tab. 2. The results suggest that our approach can be scaled to other object categories.

$\alpha$	PCK@2.5 %	PCK@5 %	PCK@10 %
VU-Net [8]	31.64	54.90	80.83
Lorenz et al. [25]	14.50	37.50	69.63
Ours	<b>41.56</b>	<b>65.76</b>	<b>83.12</b>

Table 3: **Evaluating Shape Consistency**. Percentage of Correct Keypoints (PCK) for pose estimation on shape/appearance swapped generations for supervised and unsupervised methods.  $\alpha$  is pixel distance divided by image diagonal. Note that [8] serves as upper bound, as it uses the groundtruth shape estimates.

#### 4.1 Part-based Appearance Transfer

We explore the capabilities of part-based appearance transfer between instances in Fig. 7. Parts which are transferred are displayed in color (active), parts which are not transferred are displayed in gray (inactive). The transfer succeeds despite strong occlusions and pose variations. In the most extreme case, occluded appearances can be inferred from partial observations, for instance when transferring from half-body images to full-body images or from frontal to side-ways poses. Note that we do not use any adversarial training, which causes our generated images to look rather smooth and untextured in comparison to state-of-the art image synthesis.

Following [25], we evaluate the resulting pose consistency when transferring parts between instances by calculating the percentage of correct keypoints after swapping the appearance. The results in Tab. 3 show that our method performs significantly better than [25] and even outperforms the supervised baseline VU-Net [8] by a small margin.

Due to space constraints, we refer the reader to the supplementary materials regarding an ablation study.

## 5 Conclusion

We have shown that we can build a generative model for part segmentations by a suitable combination of priors. Since the method is generative, it allows learning part segmentations without explicit supervision. Experiments demonstrate the benefits of this approach over models which obtain part masks through keypoints. Overall, this work shows that disentanglement serves as a powerful substitute for supervision and, when combined with appropriate priors, allows to directly discover part segmentations. This is in contrast to most previous works on unsupervised learning, which consider unsupervised learning merely as a pre-training step to be followed by supervised training to obtain the final result.

## 6 Acknowledgements

This work has been supported in part by the BW Stiftung project “MULT!nano”, the German Research Foundation (DFG) project 421703927, and the German federal ministry BMWi within the project “KI Absicherung”.

## References

1. Arbelaez, P.: Boundary extraction in natural images using ultrametric contour maps. In: 2006 Conference on Computer Vision and Pattern Recognition Workshop (CVPRW'06). pp. 182–182. IEEE (2006)
2. Belghazi, M.I., Baratin, A., Rajeswar, S., Ozair, S., Bengio, Y., Courville, A., Hjelm, R.D.: Mine: Mutual information neural estimation. ArXiv Prepr. ArXiv180104062 (2018)
3. Belghazi, M.I., Baratin, A., Rajeswar, S., Ozair, S., Bengio, Y., Courville, A., Hjelm, R.D.: MINE: Mutual Information Neural Estimation. ArXiv180104062 Cs Stat (Jan 2018), <http://arxiv.org/abs/1801.04062>
4. Bengio, Y., Léonard, N., Courville, A.: Estimating or Propagating Gradients Through Stochastic Neurons for Conditional Computation. ArXiv13083432 Cs (Aug 2013), <http://arxiv.org/abs/1308.3432>
5. Denton, E.L., et al.: Unsupervised learning of disentangled representations from video. In: Advances in Neural Information Processing Systems. pp. 4414–4423 (2017)
6. Eastwood, C., Williams, C.K.I.: A framework for the quantitative evaluation of disentangled representations. In: International Conference on Learning Representations (2018), <https://openreview.net/forum?id=By-7dz-AZ>
7. Esser, P., Haux, J., Ommer, B.: Unsupervised robust disentangling of latent characteristics for image synthesis. In: Proceedings of the Intl. Conf. on Computer Vision (ICCV) (2019)
8. Esser, P., Sutter, E., Ommer, B.: A Variational U-Net for Conditional Appearance and Shape Generation. arXiv:1804.04694 [cs] (Apr 2018)
9. Goodfellow, I., Pouget-Abadie, J., Mirza, M., Xu, B., Warde-Farley, D., Ozair, S., Courville, A., Bengio, Y.: Generative adversarial nets. In: Advances in Neural Information Processing Systems. pp. 2672–2680 (2014)
10. Güler, R.A., Neverova, N., Kokkinos, I.: Densepose: Dense human pose estimation in the wild. In: Proceedings of the IEEE Conference on Computer Vision and Pattern Recognition. pp. 7297–7306 (2018)
11. He, K., Zhang, X., Ren, S., Sun, J.: Delving Deep into Rectifiers: Surpassing Human-Level Performance on ImageNet Classification. arXiv:1502.01852 [cs] (Feb 2015)
12. Hung, W.C., Jampani, V., Liu, S., Molchanov, P., Yang, M.H., Kautz, J.: SCOPS: Self-Supervised Co-Part Segmentation. ArXiv190501298 Cs (May 2019), <http://arxiv.org/abs/1905.01298>
13. Hyvärinen, A., Pajunen, P.: Nonlinear independent component analysis: Existence and uniqueness results. Neural Netw. Off. J. Int. Neural Netw. Soc. **12** **3**, 429–439 (1999)
14. Jakab, T., Gupta, A., Bilen, H., Vedaldi, A.: Unsupervised learning of object landmarks through conditional image generation. In: Advances in Neural Information Processing Systems. pp. 4016–4027 (2018)
15. Jang, E., Gu, S., Poole, B.: Categorical Reparameterization with Gumbel-Softmax. ArXiv161101144 Cs Stat (Nov 2016), <http://arxiv.org/abs/1611.01144>
16. Johnson, J., Alahi, A., Fei-Fei, L.: Perceptual Losses for Real-Time Style Transfer and Super-Resolution. arXiv:1603.08155 [cs] (Mar 2016)
17. Kingma, D.P., Ba, J.: Adam: A Method for Stochastic Optimization. ArXiv14126980 Cs (Dec 2014), <http://arxiv.org/abs/1412.6980>
18. Kingma, D.P., Welling, M.: Auto-encoding variational bayes. ArXiv Prepr. ArXiv13126114 (2013)

19. Kingma, D.P., Mohamed, S., Rezende, D.J., Welling, M.: Semi-supervised learning with deep generative models. In: *Advances in Neural Information Processing Systems*. pp. 3581–3589 (2014)
20. Krähenbühl, P., Koltun, V.: Efficient Inference in Fully Connected CRFs with Gaussian Edge Potentials. *ArXiv12105644 Cs* (Oct 2012), <http://arxiv.org/abs/1210.5644>
21. Liu, R., Lehman, J., Molino, P., Such, F.P., Frank, E., Sergeev, A., Yosinski, J.: An Intriguing Failing of Convolutional Neural Networks and the CoordConv Solution. *arXiv:1807.03247 [cs, stat]* (Dec 2018)
22. Liu, Z., Luo, P., Qiu, S., Wang, X., Tang, X.: Deepfashion: Powering robust clothes recognition and retrieval with rich annotations. In: *Proceedings of IEEE Conference on Computer Vision and Pattern Recognition (CVPR)* (June 2016)
23. Liu, Z., Yan, S., Luo, P., Wang, X., Tang, X.: Fashion landmark detection in the wild. In: *European Conference on Computer Vision (ECCV)* (October 2016)
24. Locatello, F., Bauer, S., Lucic, M., Raetsch, G., Gelly, S., Schölkopf, B., Bachem, O.: Challenging common assumptions in the unsupervised learning of disentangled representations. In: *International Conference on Machine Learning*. pp. 4114–4124 (2019)
25. Lorenz, D., Bereska, L., Milbich, T., Ommer, B.: Unsupervised part-based disentangling of object shape and appearance. In: *Proceedings of the IEEE Conference on Computer Vision and Pattern Recognition (CVPR)* (2019)
26. Lu, Z., Xu, H., Liu, G.: A survey of object co-segmentation. *IEEE Access* **7**, 62875–62893 (2019). <https://doi.org/10.1109/ACCESS.2019.2917152>
27. Mathieu, M.F., Zhao, J.J., Zhao, J., Ramesh, A., Sprechmann, P., LeCun, Y.: Disentangling factors of variation in deep representation using adversarial training. In: *Advances in Neural Information Processing Systems*. pp. 5040–5048 (2016)
28. Mescheder, L., Nowozin, S., Geiger, A.: Adversarial Variational Bayes: Unifying Variational Autoencoders and Generative Adversarial Networks. *ArXiv170104722 Cs* (Jan 2017), <http://arxiv.org/abs/1701.04722>
29. Monroy, A., Ommer, B.: Beyond Bounding-Boxes: Learning Object Shape by Model-Driven Grouping. In: *Proceedings of the European Conference on Computer Vision (ECCV)*. Springer Berlin Heidelberg, Berlin, Heidelberg (2012)
30. Mumford, D.B., Shah, J.: Optimal Approximations by Piecewise Smooth Functions and Associated Variational Problems. *Commun. Pure Appl. Math.* (1989). <https://doi.org/10.1002/cpa.3160420503>, <https://dash.harvard.edu/handle/1/3637121>
31. Newell, A., Yang, K., Deng, J.: Stacked Hourglass Networks for Human Pose Estimation. *ArXiv160306937 Cs* (Mar 2016), <http://arxiv.org/abs/1603.06937>
32. Poole, B., Ozair, S., van den Oord, A., Alemi, A.A., Tucker, G.: On Variational Bounds of Mutual Information. *ArXiv190506922 Cs Stat* (May 2019), <http://arxiv.org/abs/1905.06922>
33. Ren, X., Malik, J.: Learning a classification model for segmentation. In: *Null*. p. 10. *IEEE* (2003)
34. Rezende, D.J., Mohamed, S., Wierstra, D.: Stochastic backpropagation and approximate inference in deep generative models. In: *Proceedings of the 31st International Conference on International Conference on Machine Learning-Volume 32*. pp. II–1278. *JMLR. org* (2014)
35. Rubenstein, P.K., Schoelkopf, B., Tolstikhin, I.: Learning disentangled representations with wasserstein auto-encoders (2018), <https://openreview.net/forum?id=Hy79-UJPM>

36. Rubio, J.C., Eigenstetter, A., Ommer, B.: Generative regularization with latent topics for discriminative object recognition. *Pattern Recognition* (12) (Dec 2015)
37. Singh, K.K., Ojha, U., Lee, Y.J.: FineGAN: Unsupervised hierarchical disentanglement for fine-grained object generation and discovery. In: *Proceedings of the IEEE Conference on Computer Vision and Pattern Recognition*. pp. 6490–6499 (2019)
38. Thewlis, J., Bilen, H., Vedaldi, A.: Unsupervised learning of object landmarks by factorized spatial embeddings. *ArXiv170502193 Cs Stat* (May 2017), <http://arxiv.org/abs/1705.02193>
39. Tsogkas, S., Kokkinos, I., Papandreou, G., Vedaldi, A.: Deep Learning for Semantic Part Segmentation with High-Level Guidance. *ArXiv150502438 Cs* (Nov 2015), <http://arxiv.org/abs/1505.02438>
40. Ufer, N., Ommer, B.: Deep Semantic Feature Matching. In: *2017 IEEE Conference on Computer Vision and Pattern Recognition (CVPR)*. IEEE, Honolulu, HI (Jul 2017)
41. Vicente, S., Rother, C., Kolmogorov, V.: Object cosegmentation. In: *CVPR 2011*. pp. 2217–2224. IEEE (2011)
42. Wang, P., Shen, X., Lin, Z., Cohen, S., Price, B., Yuille, A.: Joint Object and Part Segmentation using Deep Learned Potentials. *ArXiv150500276 Cs* (May 2015), <http://arxiv.org/abs/1505.00276>
43. Xue, T., Wu, J., Bouman, K.L., Freeman, W.T.: Visual dynamics: Probabilistic future frame synthesis via cross convolutional networks. In: *Advances In Neural Information Processing Systems* (2016)
44. Xue, T., Wu, J., Bouman, K.L., Freeman, W.T.: Visual dynamics: Stochastic future generation via layered cross convolutional networks. *IEEE Transactions on Pattern Analysis and Machine Intelligence (TPAMI)* **41**(9), 2236–2250 (2019)
45. Yarlagadda, P., Ommer, B.: From Meaningful Contours to Discriminative Object Shape. In: *Proceedings of the European Conference on Computer Vision (ECCV)*. Springer Berlin Heidelberg, Berlin, Heidelberg (2012)
46. Yi, K.M., Trulls, E., Lepetit, V., Fua, P.: Lift: Learned invariant feature transform. In: *European Conference on Computer Vision*. pp. 467–483. Springer (2016)
47. Zhang, W., Zhu, M., Derpanis, K.G.: From actemes to action: A strongly-supervised representation for detailed action understanding. In: *Proceedings of the IEEE International Conference on Computer Vision*. pp. 2248–2255 (2013)
48. Zhang, Y., Guo, Y., Jin, Y., Luo, Y., He, Z., Lee, H.: Unsupervised discovery of object landmarks as structural representations. In: *Proceedings of the IEEE Conference on Computer Vision and Pattern Recognition*. pp. 2694–2703 (2018)

## A Appendix

Operation	Input shape	Output shape
Input	(1, 1, 256)	(1, 1, 256)
$1 \times 1$ Conv2D	(1, 1, 256)	(1, 1, 4096)
Conv2D	(4, 4, 256)	(4, 4, 256)
residual block	(4, 4, 256)	(4, 4, 256)
residual block	(4, 4, 256)	(4, 4, 256)
Upsample	(4, 4, 256)	(8, 8, 128)
residual block	(8, 8, 128)	(8, 8, 128)
Upsample	(8, 8, 128)	(16, 16, 128)
residual block	(16, 16, 128)	(16, 16, 128)
Upsample	(16, 16, 32)	(32, 32, 32)
residual block	(32, 32, 32)	(32, 32, 32)
Upsample	(32, 32, 32)	(64, 64, 32)
residual block	(64, 64, 32)	(64, 64, 32)
Upsample	(64, 64, 32)	(128, 128, 16)
residual block	(128, 128, 16)	(128, 128, 16)
residual block	(128, 128, 16)	(128, 128, 16)
Conv2D	(128, 128, 16)	(128, 128, $n_{out}$ )

Table 4:  $D_m$  architecture.  $n_{out}$  was set to the maximum number of parts discovered. All Conv2D layer are coord-convs [21].

### A.1 Implementation Details

The neural networks used in our model are provided in Tab. 4, Tab. 5 and Tab. 6. All Conv2D layers use filters of size  $3 \times 3$ . A residual block with input  $x$  and output  $y$  is defined as follows:

$$a(x) = \text{leaky\_relu}(x) \tag{14}$$

$$y = \text{conv2D}(a(x)) + x. \tag{15}$$

A residual block with input  $x$ , incoming skip-connections  $i$  and output  $y$  is defined as follows:

$$a(x) = \text{leaky\_relu}(x) \tag{16}$$

$$c = [a(x), 1 \times \text{conv2D}(a(i))] \tag{17}$$

$$y = \text{conv2D}(c) + x. \tag{18}$$

For all experiments, the same architectures were used. All networks were initialized using the standard initialization introduced by [11]. The input images were resized to a shape of  $128 \times 128$ . The *Number of parts* - parameter  $N$  is set to an arbitrary number that is sufficiently high and provides an upper bound on the

Operation	Input shape	Output shape
Input	(128, 128, 3)	(128, 128, 3)
Conv2D	(128, 128, 3)	(128, 128, 16)
residual block	(128, 128, 16)	(128, 128, 16)
Conv2D with stride 2	(128, 128, 16)	(64, 64, 32)
residual block	(64, 64, 32)	(64, 64, 32)
Conv2D with stride 2	(64, 64, 32)	(32, 32, 64)
residual block	(32, 32, 64)	(32, 32, 64)
Conv2D with stride 2	(32, 32, 64)	(16, 16, 128)
residual block	(16, 16, 128)	(16, 16, 128)
Conv2D with stride 2	(16, 16, 128)	(8, 8, 128)
residual block	(8, 8, 128)	(8, 8, 128)
Conv2D with stride 2	(8, 8, 128)	(4, 4, 256)
residual block	(4, 4, 256)	(4, 4, 256)
4× residual block	(4, 4, 256)	(4, 4, 256)
mean pooling	(4, 4, 256)	(1, 1, 256)
1 × 1 Conv2D	(1, 1, 256)	(1, 1, $n_{out}$ )

Table 5:  $E_\alpha$  and  $E_\beta$  architectures. For  $E_\beta$ , we use coord-convs [21]. This means that we additionally concatenate the spatial coordinates to the feature maps before convolution.  $n_{out}$  is 256 for  $E_\beta$  and 64 for  $E_\alpha$ .

Operation	Input shape	Output shape
Input	(128, 128, 89)	(128, 128, 89)
Conv2D	(128, 128, 89)	(128, 128, 32)
residual block	(128, 128, 32)	(128, 128, 32)
Conv2D with stride 2	(128, 128, 32)	(64, 64, 64)
residual block (a)	(64, 64, 64)	(64, 64, 64)
residual block	(64, 64, 64)	(64, 64, 64)
residual block with skip from (a)	$2 \times (64, 64, 64)$	(64, 64, 64)
Upsample bilinear	(128, 128, 32)	(128, 128, 32)
residual block	(128, 128, 32)	(128, 128, 32)
Conv 2D	(128, 128, 32)	(128, 128, 3)

Table 6:  $G$  architecture, resembling a shallow hourglass network. Incoming skip connections are first passed through the activation function, then convolved with a  $1 \times 1$ -conv2D and then concatenated to the input from the upsampling stage.

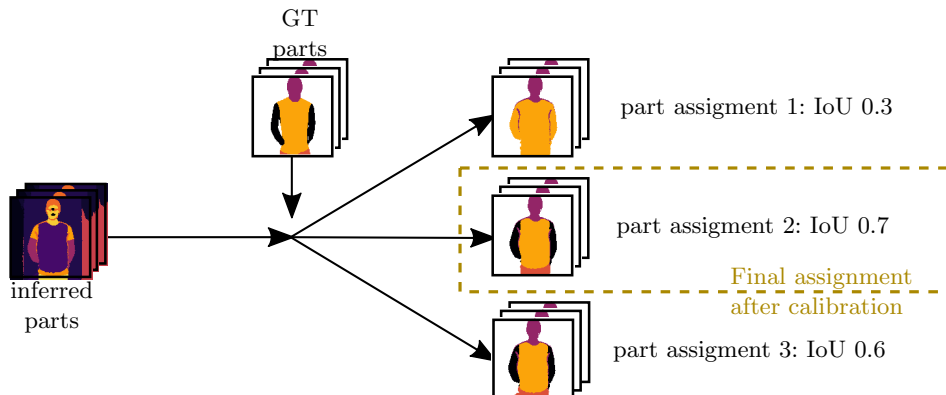


Fig. 8: **Calibration Step.** Given the set of inferred parts, the calibration step calculates the IoU with each possible assignment of individual ground-truth parts. Afterwards, the assignment with the best IoU score is used for evaluation.

discovered parts. We choose 25 for all experiments, without loss of generality. We apply no data augmentation other than horizontal flipping. We train our model with batch size 4 for 100 000 steps using the Adam optimizer [17] with an initial learning rate of  $2 \cdot 10^{-4}$ .  $I_T$  is calculated with an exponential moving average with a decay of 0.99. The value of  $\lambda_{\text{GMRF}}$  is set to  $1.0 \cdot 10^{-3}$ . The value of  $\lambda_{H(p)}$  is set to  $0.06 \cdot 10^{-3}$  at the beginning of the training and linearly increased between 30 000 and 50 000 steps to 0.06. The dimensionalities of latent variables are:  $\dim(\alpha) = 128$  and  $\dim(\pi) = 64$ .

We provide details on the datasets that were used in our experiments:

**Deepfashion** We use the train and test split provided by [22, 23], consisting of 31 802 for training and 984 for testing.

**Pennaaction** We use a subset of the train and test split provided by [47], consisting of 1648 for training and 1689 for testing.

**CUB** We use the train and test split provided by [25], consisting of 4736 images for training and 4631 for testing.

## A.2 Keypoint Baselines, Postprocessing and Calibration Step

We highlight details on how we compare the results of unsupervised keypoint estimation baselines [14, 25, 48] with our results on unsupervised segmentation baselines. We trained all unsupervised keypoint baseline with the same number of parts (25) and the same input image size ( $128 \times 128$ ) as we trained our model.

*Calibration Step* The calibration step is depicted in Fig. 8. Given a set of inferred segmentations with paired ground-truth segmentations, the IoU for all possible assignments from inferred segmentations to ground-truth segmentations is calculated. Finally, the assignment with best IoU chosen.

Dataset	Method	$\sigma$	Arms	Feet	Head	Legs	Torso	Overall
DeepFashion	[48]	0.010	0.006	0	0.014	0.000	0.008	0.006
DeepFashion	[48]	0.050	<u>0.232</u>	0	0.579	0.296	0.307	0.283
DeepFashion	[48]	0.100	0.194	0	<u>0.598</u>	0.293	<u>0.376</u>	0.292
DeepFashion	[14]	0.010	0.002	0	0.001	0.000	0.004	0.001
DeepFashion	[14]	0.050	0.002	0	0.042	0.056	0.088	0.038
DeepFashion	[14]	0.100	0.052	0	0.118	0.108	0.244	0.104
DeepFashion	[25]	0.010	0.002	0	0.009	0.000	0.014	0.005
DeepFashion	[25]	0.050	0.107	0	0.272	0.181	0.318	0.176
DeepFashion	[25]	0.100	0.215	0	<b>0.606</b>	<u>0.309</u>	0.322	<u>0.290</u>
DeepFashion	Ours	-	<b>0.508</b>	0.000	0.530	<b>0.500</b>	<b>0.722</b>	<b>0.452</b>
Exercise	[48]	0.010	0.004	0.086	0.016	0.032	0.201	0.068
Exercise	[48]	0.050	0.041	<b>0.226</b>	0.103	0.428	0.333	0.226
Exercise	[48]	0.100	0.023	0.065	0.021	0.250	0.241	0.120
Exercise	[14]	0.010	0.000	0.055	0.000	0.132	0.275	0.092
Exercise	[14]	0.050	0.091	0.175	0.103	<u>0.462</u>	0.380	0.222
Exercise	[14]	0.100	0.098	0.192	0.000	<b>0.464</b>	0.350	0.221
Exercise	[25]	0.010	0.134	0.146	<b>0.395</b>	0.332	0.428	0.287
Exercise	[25]	0.050	0.212	<u>0.213</u>	<u>0.363</u>	0.432	<u>0.437</u>	<b>0.332</b>
Exercise	[25]	0.100	<u>0.218</u>	0.204	0.305	0.433	0.430	0.318
Exercise	Ours	-	<b>0.253</b>	0.104	0.340	0.428	<b>0.504</b>	<u>0.326</u>

Table 7: Segmentation IOU for each unsupervised keypoint baseline + CRF [20] on each dataset. Bold means best, underlined means second best. The IOU performance strongly depends on the chosen variance of the isotropic Gaussian that models the extent of the keypoints. As one can see, taking a good hyperparameter from one dataset to another is not possible. Our proposed method does not rely on postprocessing and therefore is consistent across datasets.

*Postprocessing of Keypoint Baselines* To transform keypoints into segmentations, we create an isotropic Gaussian decay around each keypoint and then use it as unary potentials for a conditional random field inference. We noticed that the segmentation quality strongly depends on the variance  $\sigma$  that is used to create the Gaussian decay.

We therefore optimized this parameter over a range of  $\sigma$  parameters to find good segmentation in terms of final IOU with the ground-truth on the validation set. To calculate the IOU, we apply the calibration step as described above. We do this for each baseline and on each dataset individually and always select the *best parameter configuration* based on overall IOU performance. We do not apply any postprocessing on our results.

For completeness, we report the full table of segmentation results in Tab. 7. We observe that choosing a good hyperparameter for the variance of the Gaussian decay does not generalize across methods and datasets. For DeepFashion, the variance in terms of IOU performance is very high. We argue that this is because of the strong appearance variation of the dataset. As already described, our method explicitly factors out some variation of the appearance by limiting the mutual information. Therefore, our method works much better under such circumstances. The effect is not as strong on exercise due to simple part appearances such as blue shirt, black sports pants, etc. Therefore, a good segmentation can be achieved using only the CRF and keypoints.

### A.3 Additional Qualitative Results

We show additional qualitative results for comparison against keypoint-based baselines. Results for DeepFashion are shown in Fig. 9, for Exercise in Fig. 10 and for Pennaction in Fig. 11. It can clearly be seen that our method discovers parts which are consistent across instances and poses. Furthermore, discovered keypoints are hard to assign to semantic parts.

### A.4 Derivation for Gaussian Markov Random Field

For completeness, we derive (9). For some parameter  $\mathbf{y}$ , a prior  $p(\mathbf{y})$  is chosen as an improper GMRF with zero mean.

$$p(\mathbf{y}) = \mathcal{N}(\mathbf{0}, \mathbf{Q}^{-1}), \quad \mathbf{Q}^{\frac{1}{2}} = \nabla \quad (19)$$

Then, the posterior  $p(\mathbf{y} | \mathbf{x})$  is inferred from a different random variable  $\mathbf{x}$ . In a variational inference framework, the posterior is now assumed to be an isotropic Gaussian around an inferred mean  $f(\mathbf{x})$ .

$$q(\mathbf{y} | \mathbf{x}) = \mathcal{N}(f(\mathbf{x}), \mathbf{I}) \quad (20)$$

By regularizing the KL between  $q$  and  $p$ , the posterior is kept close to the prior. With the chosen  $q$  and  $p$ , we get:

$$p(\mathbf{y}) = \mathcal{N}(\mathbf{0}, \mathbf{Q}^{-1}), \quad \mathbf{Q}^{\frac{1}{2}} = \nabla \quad (21)$$

$$q(\mathbf{y} | \mathbf{x}) = \mathcal{N}(f(\mathbf{x}), \mathbf{I}) \quad (22)$$

$$\mathcal{N}_0 = \mathcal{N}(\boldsymbol{\mu}_0, \Sigma_0), \quad \mathcal{N}_1 = \mathcal{N}(\boldsymbol{\mu}_1, \Sigma_1) \quad (23)$$

$$\text{KL}(\mathcal{N}_0 \| \mathcal{N}_1) = \frac{1}{2} \left[ \text{tr}(\Sigma_1^{-1} \Sigma_0) + (\boldsymbol{\mu}_1 - \boldsymbol{\mu}_0)^{\text{T}} \Sigma_1^{-1} (\boldsymbol{\mu}_1 - \boldsymbol{\mu}_0) + \text{const} \right] \quad (24)$$

$$\text{KL}(q \| p) = \frac{1}{2} \left[ \underbrace{\text{tr}(\mathbf{Q}\mathbf{I})}_{\text{const}} + \underbrace{f(\mathbf{x})^{\text{T}} \mathbf{Q} f(\mathbf{x})}_{\left\| \mathbf{Q}^{\frac{1}{2}} f(\mathbf{x}) \right\|^2} + \text{const} \right] = \lambda \|\nabla f(\mathbf{x})\|^2 + \text{const}. \quad (25)$$

Observe that the KL boils down to the gradient of  $f(\mathbf{x})$ , which in practice has to be approximated by finite differences. If  $f(\mathbf{x})$  is a 2D tensor for example, it is simply the image gradient.

### A.5 Part-based Appearance Transfer

We show high resolution versions of Fig. 7 in Fig. 12, Fig. 13, Fig. 14, Fig. 15.

### A.6 Ablation Studies

We conduct an ablation study in Fig. 16. To start simple, we use a model without disentanglement, GMRF prior or entropy regularization. We expect this model to fail, since there is no incentive to factorize the distribution into independent shape and appearance representations. The model diverges after roughly 3000 steps.

We introduce disentanglement by adding variational and adversarial objectives. This prevents the model from diverging, however it converges to a an undesired local minimum consisting of a single constant part.

We now constrain the solutions of  $S$  by adding the GMRF prior, which clearly encourages localized parts to be discovered.

Adding the entropy regularization objective increases the smoothness of our solution.

Finally we ask the question if we really need variational and adversarial objectives or if either of them is sufficient. We expect this model to take into account appearance cues such as average color, instead of semantic consistency across instances when factorizing the data distribution. The experiment validates this hypothesis as the torso parts are not consistently labelled as the same part, which previously has been the case.

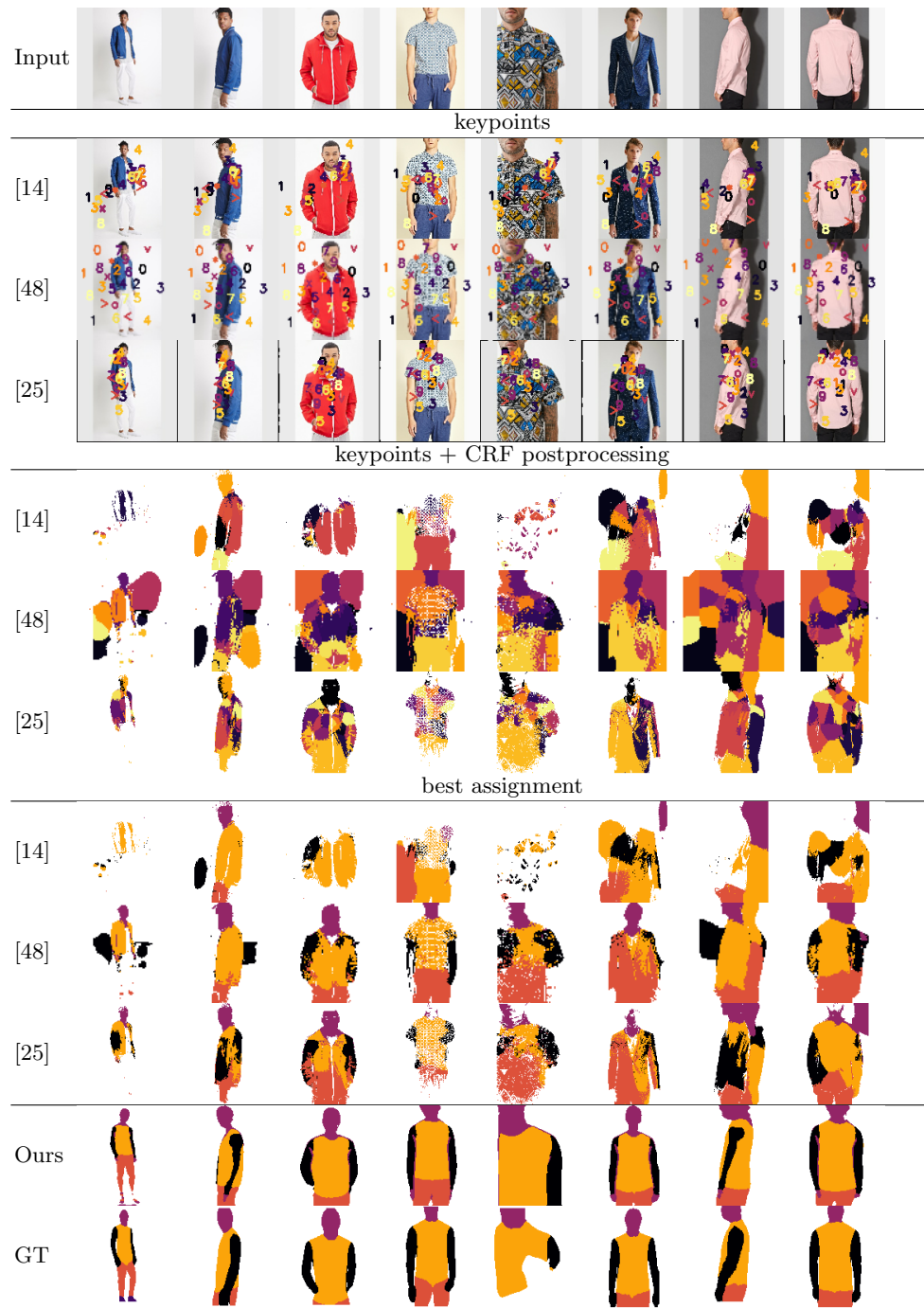


Fig. 9: Additional results for comparison against keypoint-based baselines on DeepFashion.

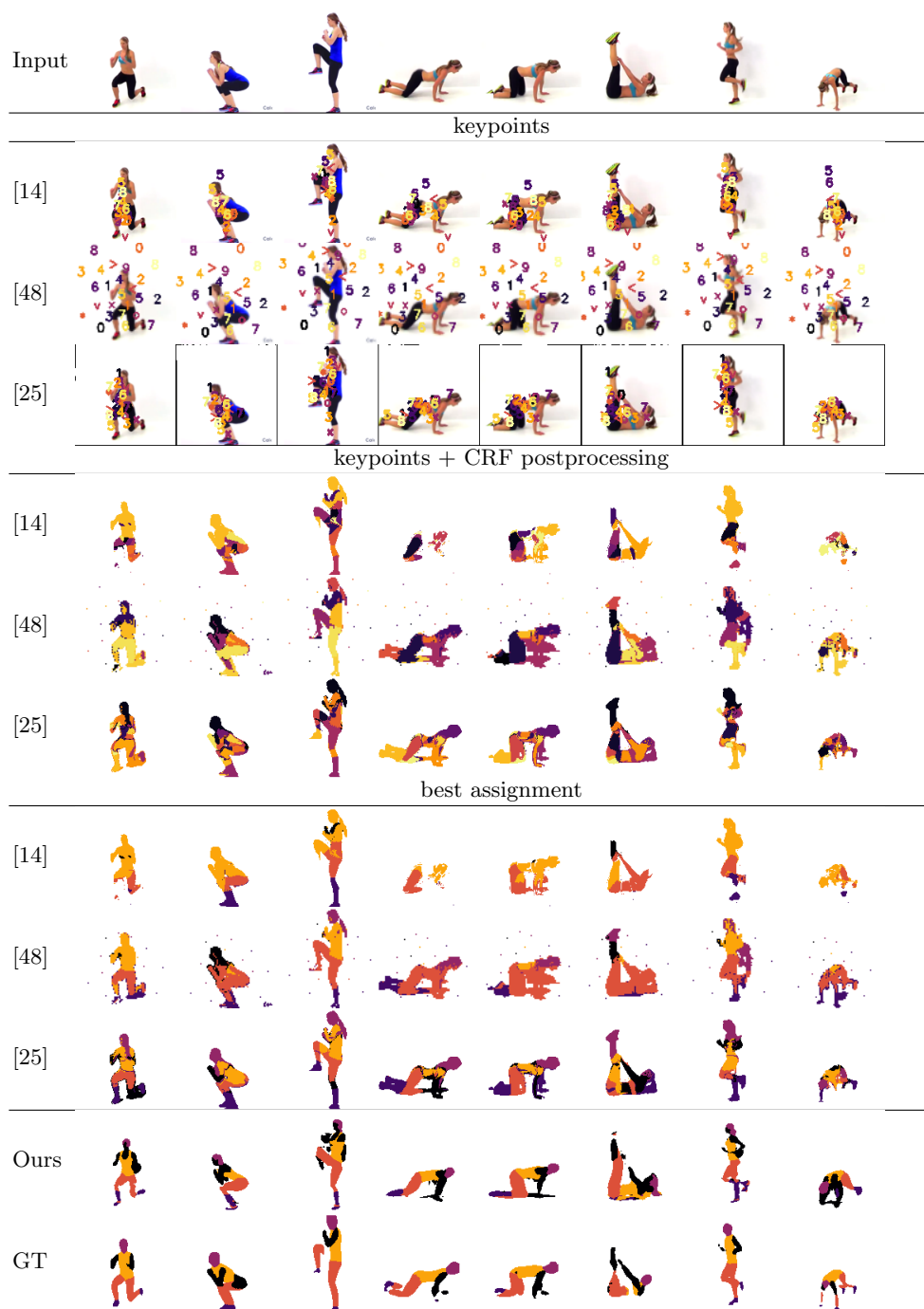


Fig. 10: Additional results on Exercise.

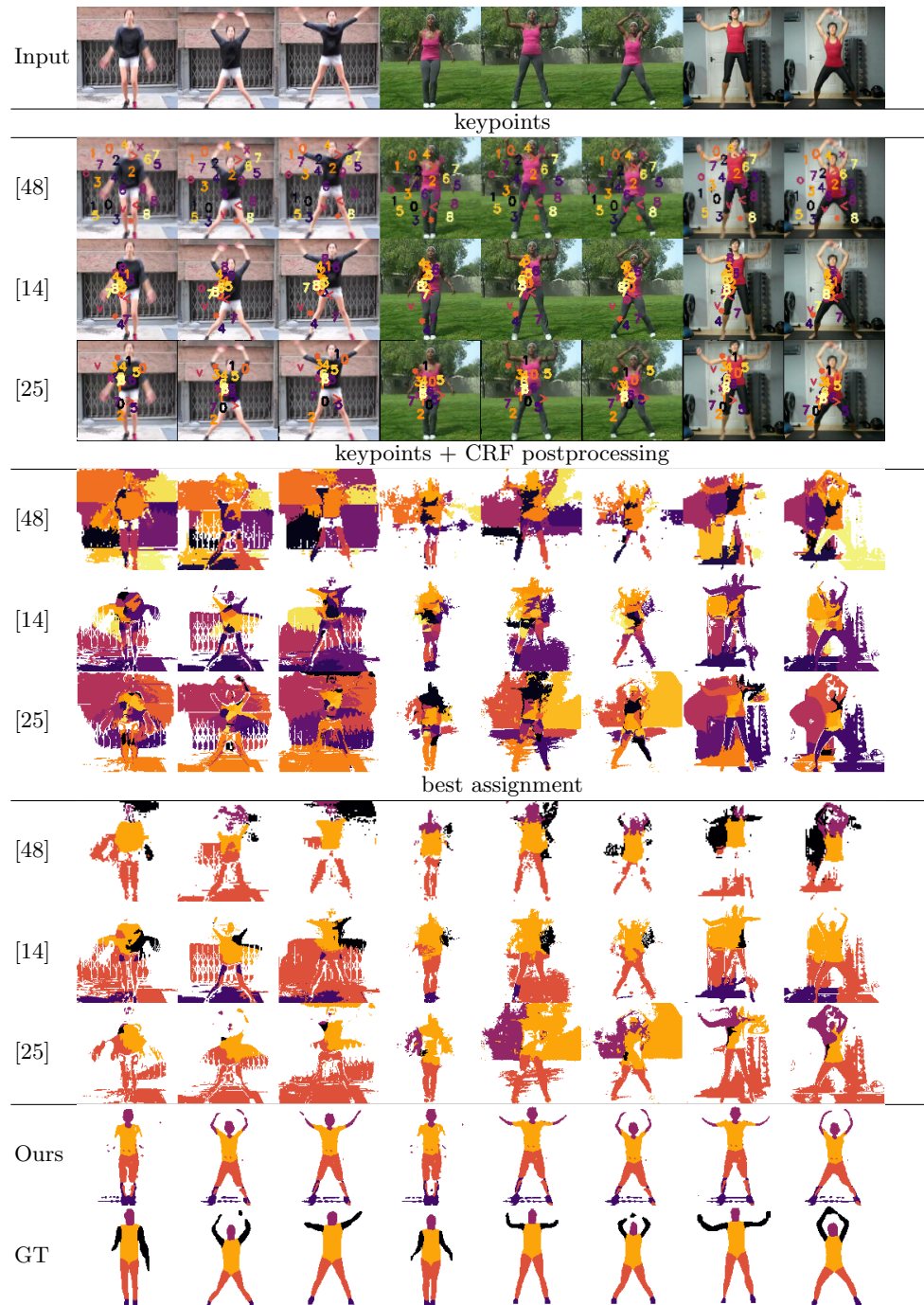


Fig. 11: Additional results on Pennaction.

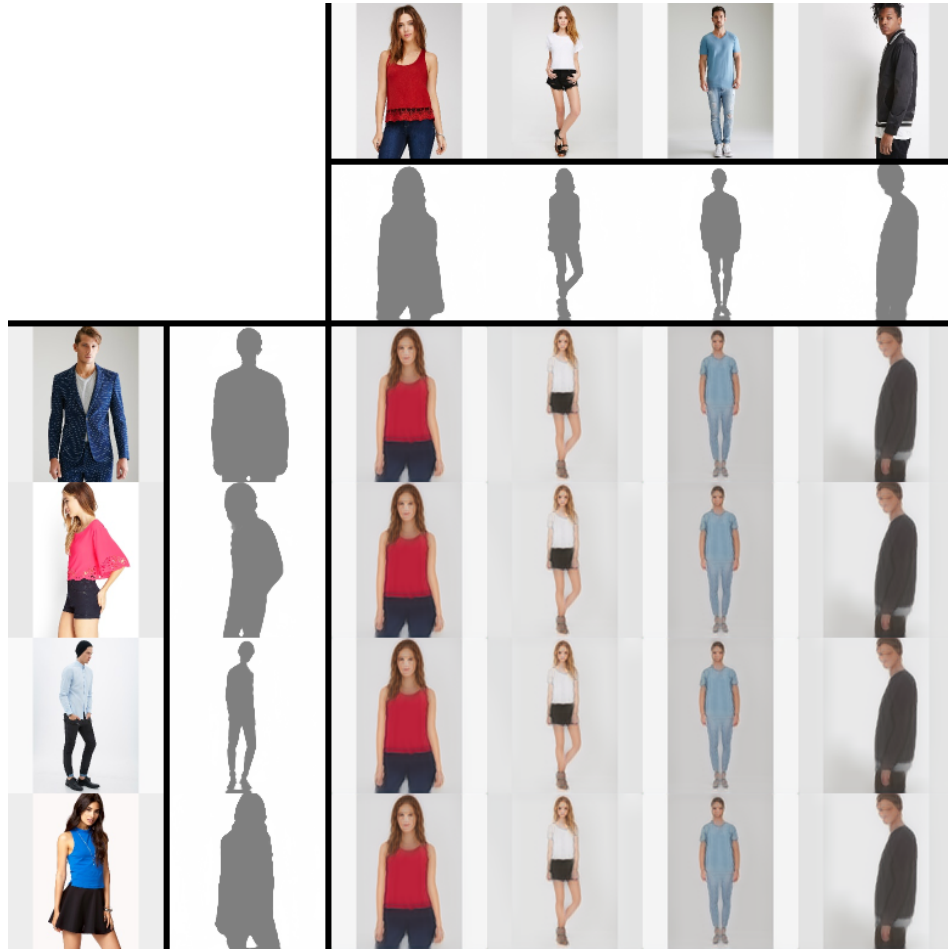


Fig. 12: **Part-based Appearance Transfer**. No Swaps applied.

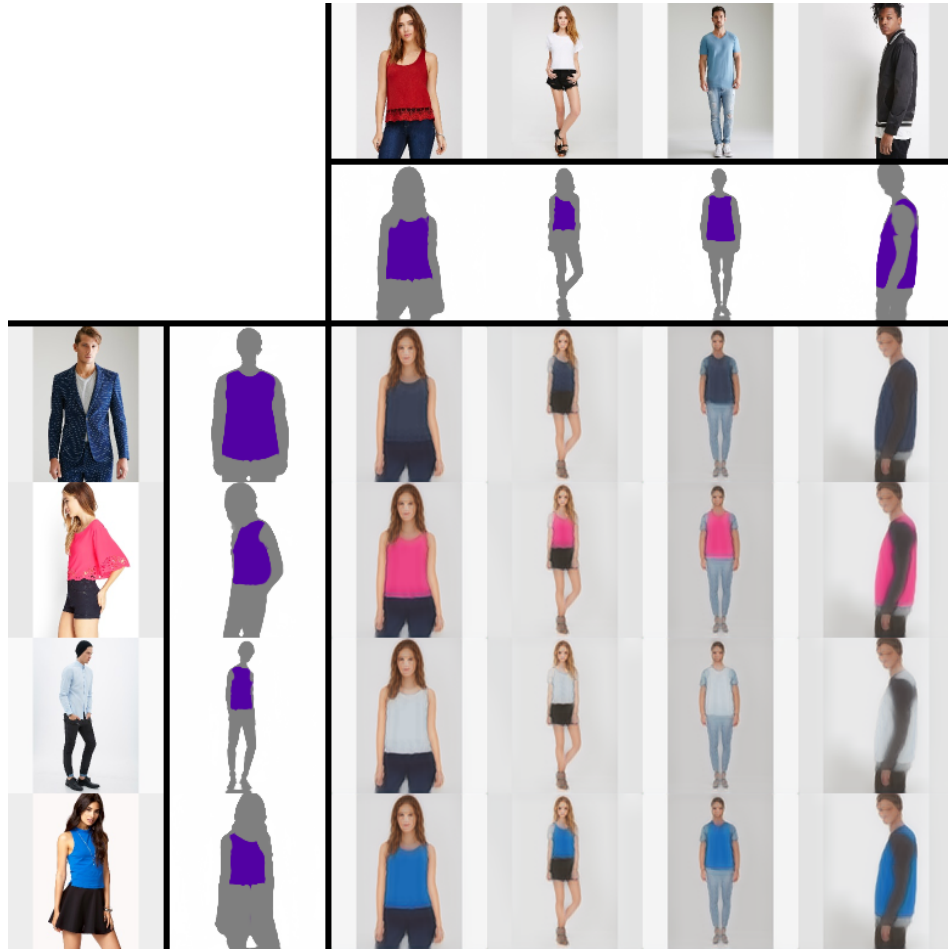


Fig. 13: **Part-based Appearance Transfer.** Swapping only chest appearance.



Fig. 14: Part-based Appearance Transfer. Swapping chest and arm appearance.

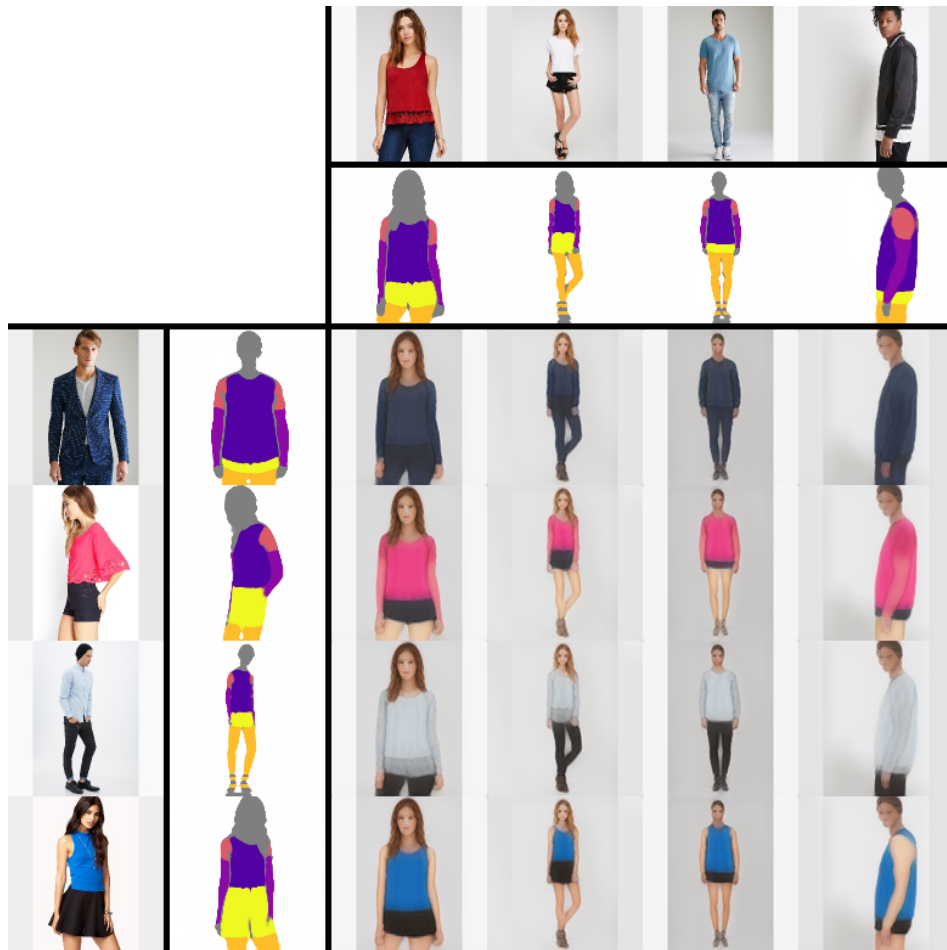


Fig. 15: **Part-based Appearance Transfer**. Swapping chest, arm, hip and leg appearance.

	disentanglement	GMRF	$\mathcal{L}_{H(p)}$			
1.	$\times$	$\times$	$\times$			
2.	variational + adversarial	$\times$	$\times$			
3.	variational + adversarial	$\checkmark$	$\times$			
4.	only variational	$\checkmark$	$\checkmark$			
5.	Full Model, variational + adversarial	$\checkmark$	$\checkmark$			

Fig. 16: **Analyzing Disentanglement, GMRF prior and Entropy Regularization.** We highlight the importance of each introduced prior in a series of ablation studies.